The Astrophysical Journal, 587:117–122, 2003 April 10

RESOLVED MID-INFRARED EMISSION IN THE NARROW-LINE REGION OF NGC 4151

James T. Radomski, Robert K. Piña, Christopher Packham, and Charles M. Telesco
Department of Astronomy, University of Florida, Gainesville, FL 32611

James M. De Buizer
Cerro Tololo Inter-American Observatory (CTIO), National Optical Astronomy Observatory, 603 Casilla, La Serena, Chile

R. Scott Fisher
Gemini Observatory, Northern Operations Center, 670 North A'ohoku Place, Hilo, HI 96720

and

A. Robinson
Department of Physical Sciences, University of Hertfordshire, College Lane, Hartfield, Hertfordshire AL10 9AB, UK
Received 2002 August 21; accepted 2002 November 26

ABSTRACT

We present subarcsecond-resolution mid-infrared images of NGC 4151 at 10.8 and 18.2 μm. These images were taken with the University of Florida mid-IR camera/spectrometer OSCIR at the Gemini North 8 m telescope. We resolve emission at both 10.8 and 18.2 μm, extending $\sim 3\farcs5$ across at a P.A. of $\sim 60^\circ$. This coincides with the narrow-line region of NGC 4151, as observed in [O III] by the *Hubble Space Telescope*. The most likely explanation for this extended mid-IR emission is dust in the narrow-line region heated by a central engine. We find no extended emission associated with the proposed torus and place an upper limit on its mid-IR size of $\lesssim 35$ pc.

Subject headings: galaxies: individual (NGC 4151) — galaxies: Seyfert — infrared: galaxies

1. INTRODUCTION

NGC 4151 is one of the nearest (13.2 Mpc, $H_0 = 75$ km s^{-1} Mpc^{-1}) and best-studied active galactic nuclei (AGN). The nucleus hosts a highly variable continuum and line emission source. Continuum variability, first reported by Fitch, Pacholczyk, & Weymann (1967), has been observed at several wavelengths, including X-ray (Papadakis & McHardy 1995), UV (Clavel et al. 1990), and optical (Lyutyi 1972). Classified as a Seyfert 1.5 nucleus by Osterbrock & Koski (1976), NGC 4151 displayed characteristics of a Seyfert 2 nucleus (Penston & Pérez 1984) during a low-luminosity state in 1984 and, at a later date, characteristics of a Seyfert 1 galaxy (Ayani & Maehara 1991).

The mid-infrared emission from NGC 4151 has been suggested as arising from either thermal emission from dust grains or synchrotron emission. Discussions of the thermal versus nonthermal origin of the infrared emission in NGC 4151 can be found in Rieke & Lebofsky (1981), Edelson & Malkan (1986), Carelton et al. (1987), Edelson, Malkan, & Rieke (1987), and de Kool & Begelman (1989). A direct method to investigate the origin of the mid-IR emission mechanism, as proposed by Neugebauer et al. (1990, hereafter N90), is a measurement of the size of the emitting region. They suggest that a nonthermal self-absorbed synchrotron source would be less than 1 mas and hence unresolvable. However, if the mid-IR emission is due to heated dust grains, the size of the region would be greater than $0\farcs1$.

Observations show that the mid-IR emission in NGC 4151 is compact. Comparison between $60''$ resolution *IRAS* 12 μm flux density measurements and $6''$ resolution ground-based 10.6 μm measurements agree to within $\sim 6\%$ (Edelson et al. 1987). Mid-IR observations by Rieke & Low (1972), Rieke & Lebofsky (1981), and Ward et al. (1987) also did not detect any extended emission with resolutions $\gtrsim 6''$. Observations by the *Infrared Space Observatory* (*ISO*; Rodriquez-Espinosa et al. 1996, hereafter RE96) show a strong warm dust component in NGC 4151 and suggest a thermal origin from a geometrically and optically thick dusty torus and/or a dusty narrow-line region (NLR). These observations, however, were at a resolution of $180''$. Using a technique of near-simultaneous north-south scans at 2.2 and 11.2 μm, N90 was able to resolve the 11.2 μm emitting region to be $0\farcs16 \pm 0\farcs04$. However, this technique measured the size in only one spatial direction and was insufficient to explore the mid-IR morphology of the circumnuclear region. In addition, these north-south scans could not investigate the NLR of NGC 4151, which is primarily orientated in an east-west direction. In this paper we present high-resolution mid-IR imaging, which, to the best of our knowledge, resolves the inner NLR of NGC 4151 for the first time at 10 and 18 μm.

2. OBSERVATIONS AND DATA REDUCTION

Observations of NGC 4151 were made on 2001 May 7 using the University of Florida mid-infrared camera/spectrometer OSCIR on the Gemini North 8 m telescope. OSCIR uses a Rockwell 128 × 128 Si:As Blocked Impurity Band (BIB) detector. On Gemini North, OSCIR has a plate scale of $0\farcs089$ pixel^{-1}, corresponding to a field of view of $11\farcs4 \times 11\farcs4$. Images were obtained in the N ($\lambda_0 = 10.8$ μm, $\Delta\lambda = 5.2$ μm) and IHW18 ($\lambda_0 = 18.2$ μm, $\Delta\lambda = 1.7$ μm) filters using a standard chop-nod technique to remove sky background and thermal emission from the telescope. The chopper throw was $15''$ in declination at a frequency of 3 Hz, and the telescope was nodded every 30 s.

NGC 4151 was observed for a total chopped integration time of 360 s at 10.8 μm and 480 s at 18.2 μm. Observations of β Gem were taken for flux calibration and as a measure of the telescope point-spread function (PSF). Measure-

ments of other calibration stars throughout the night showed flux calibration variations of less than 5% at 10.8 μm and less than 10% at 18.2 μm. Absolute calibration of β Gem was achieved using a spectral irradiance model by Cohen et al. (1995) adjusted for filter and atmospheric transmission. The calibration value and FWHM were also color-corrected to account for the different spectral slope of β Gem versus NGC 4151, as observed within our N and IHW18 filters. The measured color-corrected FWHM of β Gem was 0.″53 at 10.8 μm and 0.″58 at 18.2 μm based on a 60 s chopped integration. Short integrations of β Gem were sufficient for comparison to NGC 4151 due to the stability of the OSCIR/Gemini PSF. Observations of several standard stars, including β Gem, μ UMa, and γ Aql, showed variations in the FWHM of less than 6% throughout the night. Finally, observations of NGC 4151 showed no change in structure when divided into increments of time equal to that of the PSF (60 s).

OSCIR was mounted on the telescope with the Gemini instrument rotator oriented such that north was up and east was left on the detector array. In postprocessing, images of the PSF star β Gem were "unrotated" $-17.^{\circ}4$ and $-22.^{\circ}9$ at 10.8 and 18.2 μm, respectively, to match the position angle of the Gemini North telescope *pupil*, as projected on the detector array when NGC 4151 was observed. This is necessary to correctly account for the rotation of the telescope pupil with respect to OSCIR (during an observation or when changing pointing) due to the alt-az mount of the Gemini North telescope. In addition, PSF images were rotationally "smeared" to account for the slight rotation of the pupil ($\lesssim 4^{\circ}$) during the exposure times of NGC 4151.

Flux density maps were created by convolving images at 10.8 μm with the 18.2 μm PSF and vice versa to attain the same resolution at both wavelengths. Color temperature and emission optical depth maps were calculated based on the ratio of these images. Since no astrometric calibration was performed because of the limited field of view of OSCIR, the peak flux of the convolved 10.8 μm image was aligned to coincide with peak flux of the convolved 18.2 μm image. Temperature and emission optical depth were then calculated using the optically thin approximation $F_\nu = \Omega\tau B_\nu(T)$, where F_ν is the observed flux density at frequency ν, Ω is the solid angle of each pixel, τ is the emission optical depth, and $B_\nu(T)$ is the Planck function evaluated at frequency ν and temperature T. The structure of the temperature map was highly dependent on the alignment of the two convolved images. In order to determine the errors due to alignment, a Monte Carlo simulation was performed by shifting the two convolved images with respect to each other up to 0.″1 in all directions. Temperature values were most stable in the core varying ± 5 K, with variations of ± 15 K farther out. The frequency dependence of dust grain emission efficiency in the mid-IR was approximated as $Q(v) \propto v^1$. A steeper power-law dependence, such as $Q(v) \propto v^2$, would decrease the calculated temperatures $\sim$15% and correspondingly increases the emission optical depth by a factor of $\sim$3.4.

3. RESULTS

NGC 4151 shows extended emission $\sim$3.″5 across, oriented in an approximately east-west direction. Perpendicular to the extended emission (roughly north-south), the galaxy remains unresolved based our limiting resolution of

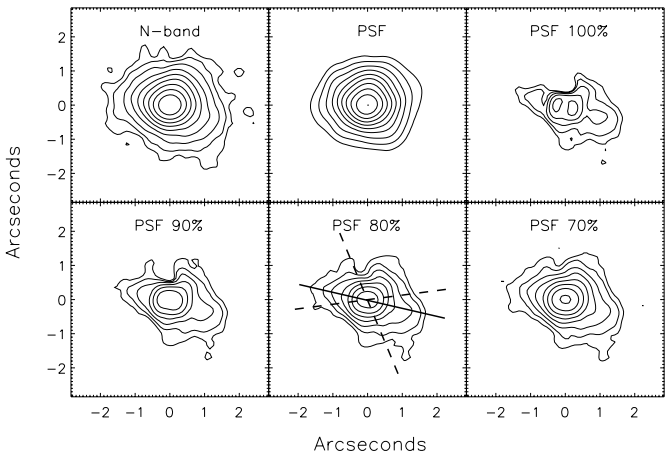

FIG. 1.—*N*-band images of the central $\sim$6″ of NGC 4151. All images are smoothed with a $\sim$0.″25 Gaussian filter to enhance low-level emission and scaled logarithmically. Contours are separated by a factor of 1.84, with the lowest contour representing the 3 σ level of the smoothed data (0.086 mJy). The next image shows the PSF star β Gem scaled to the same level as NGC 4151 for comparison. The next four images show the residuals of NGC 4151 after subtraction of the PSF (unresolved component) scaled to 100%, 90%, 80%, and 70% of the peak height. In the 80% image, dashed lines delineate the edges of the ionization region, as observed by Evans et al. (1993), while the solid line represents the radio jet axis. With the peak scaled to the same height as NGC 4151 (100%), the unresolved component represents $\sim$73% of the total emission detected at 10 μm.

$\sim$0.″53–0.″58 at 10.8 and 18.2 μm, respectively. Figure 1 shows our *N*-band image of the central $\sim$400 pc ($\sim$6″) of NGC 4151. Subtraction of the unresolved (PSF) component scaled to 100% of the peak results in a hole at the center of the residual emission. Since this may represent an oversubtraction of the unresolved component, we also show the residuals after subtraction of the PSF scaled to 90%, 80%, and 70% of the peak of NGC 4151. Figure 2 shows a similar comparison at 18.2 μm. Both figures clearly show extended mid-IR emission on a much larger scale than previously measured.

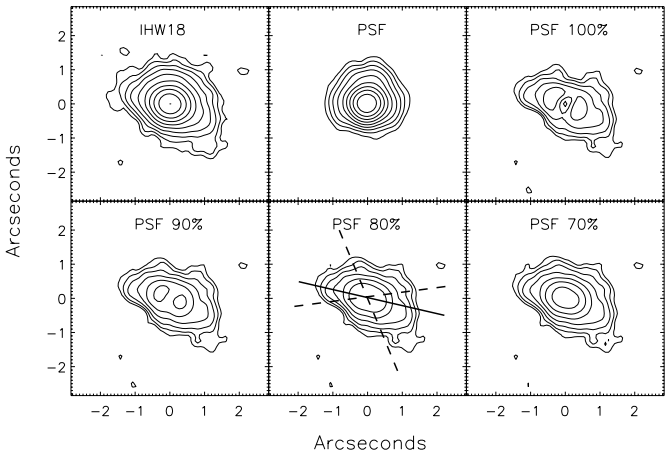

FIG. 2.—Shows IHW18 (18 μm) images of the central $\sim$6″ of NGC 4151 in the same format as Fig. 1. Contours are separated by a factor of 1.65, with the lowest contour representing the 3 σ level of the smoothed data (0.46 mJy). With the peak scaled to the same height as NGC 4151 (100%), the unresolved component represents $\sim$73% of the total emission detected at 18 μm.

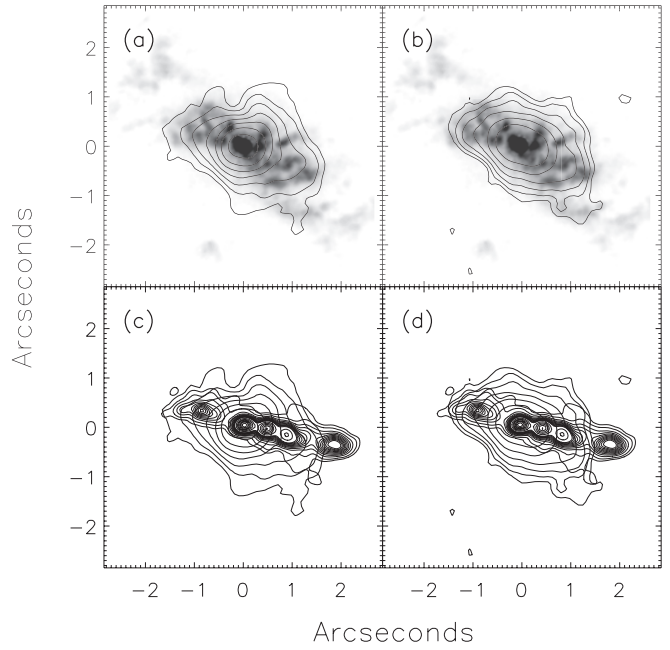

FIG. 3.—Contours represent the extended emission at *N* and IHW18 after PSF subtraction (with PSF scaled to 80% of the peak). Images (*a*) and (*b*) show the extended *N* and IHW18 emission, respectively, overlaid on the *HST* [O III] ionization region, as observed by Kaiser et al. (2000). Images (*c*) and (*d*) show the same *N* and IHW18 emission overlaid on the radio jet, as observed at 18 cm by Pedlar et al. (1998). In all images, the peak emission in the radio and [O III] are aligned to correspond with the peak in the mid-IR region.

The extent and position angle ($\sim$60°) of the extended emission is coincident with the NLR, as observed by Evans et al. (1993) and Kaiser et al. (2000), using *HST*. This NLR was resolved at [O III] λ5007 into a number of emission-line clouds distributed in a biconical structure oriented along a P.A. = 60° ± 5°, with an opening angle of 75° ± 10° (Evans et al. 1993). NGC 4151 also contains a radio jet (Johnston et al. 1982; Pedlar et al. 1993; Mundell et al. 1995), which extends along a slightly different PA ($\sim$77°) than the [O III] emission. Figure 3 shows our mid-IR images overlaid on the [O III] and radio maps in the central $\sim$6″. The extended mid-IR emission strongly coincides with the [O III] emission out to a distance of $\sim$100 pc from the nucleus on either side.

TABLE 1
NGC 4151 FLUX DENSITY MEASUREMENTS

Description	Filter	Aperture	Flux Density
Total	*N* Band	4.″5	1874 ± 52 [a]
Unresolved (≤73%)		[b]	≤1368 ± 38
Extended (≥27%)		[b]	≥506 ± 14
Long Wavelength			
Total	IHW18	4.″5	4386 ± 241[a]
Unresolved (≤73%)		[b]	≤3202 ± 176
Extended (≥27%)		[b]	≥1184 ± 65

[a] All flux densities are color-corrected and in units of mllijanksy. Errors in flux density are dominated by uncertainty in calibration (±2.5% at the *N* band and ±5% at IHW18) but also include a small statistical error based on the aperture size.

[b] Flux density measurements were performed by scaling the PSF star β Gem to 100% of the peak of NGC 4151 and subtracting off to find the contribution from the resolved and unresolved component.

As previously mentioned, north-south scans by N90 measure the 11.2 μm emitting region to be 0.″16 ± 0.″04 or $\sim$10 pc. We see no extended emission in this direction and can only place an upper limit on the mid-IR size of $\lesssim$35 pc based on our resolution limit of $\sim$0.″53–0.″58. Scaling the PSF to 100% of the peak of NGC 4151 results in an upper limit of the unresolved component of $\leq$73% of the total emission at 10.8 and 18.2 μm and a lower limit to the extended component of $\geq$27%. Table 1 shows our mid-IR flux density measurements.

4. ANALYSIS AND DISCUSSION

Based on the conclusion from N90 that a nonthermal self-absorbed synchrotron source would be less than 1 mas and hence unresolvable, our results are consistent with a thermal origin of the extended mid-IR emission. The reradiation by dust grains heated by either stars or an AGN may result in this extended thermal mid-IR emission. However, processes such as fine-structure emission lines may also produce extended mid-IR emission. Several mid-IR fine structure lines were observed by Sturm et al. (1999) using *ISO*. Four of these emission lines fall within our broadband *N* and IHW18 filters and may contribute to this mid-IR emission. These emission lines are the 8.99 μm [Ar III], 10.51 μm [S IV], 12.81 μm [Ne II], and 18.71 μm [S III]. However, based on flux measurements from Sturm et al. (1999), these emission lines contribute less than 10% of the extended emission that we observe at 10.8 and 18.2 μm.

Several mechanisms can contribute to thermal dust emission in the mid-IR. These include shock heating, in situ star formation, dust in the NLR heated by the central engine, and a dusty torus. Each is considered below in the context of the mid-IR emission that we detect in NGC 4151.

4.1. *Dust Heated in Shocks*

Shock heating of dust grains caused by the radio jet may contribute to mid-IR emission in NGC 4151. Mid-IR emission from shocks may be produced by either direct collisions between the plasma and dust particles (Draine 1981) or absorption of UV radiation produced by the postshock cooling plasma (Dopita & Sutherland 1996). However, radial velocity measurements of Kaiser et al. (2000) show no correspondence between velocity or velocity dispersion and the positions of the radio knots of NGC 4151. Models by Crenshaw et al. (2000) also do not require strong shocks to explain the kinematics of the NLR. Shocks may still contribute to the NLR, as suggested by Contini, Viegas, & Prieto (2002), but are not considered to be a major source of ionization. Recent [Fe II] observations by Turner et al. (2002) also support this concept. Thus, shock heating, although not ruled out, is not considered as a major source of the mid-IR emission that we observe.

4.2. *Star Formation*

Mid-IR emission has been observed to arise from star formation in the central regions of many galaxies (e.g., Telesco 1988). The mid-IR provides an excellent trace of H II star-forming regions whose emission peaks at far-IR wavelengths (50–200 μm). Observations by Engargiola et al. (1988) at 155 μm show extended emission (>48″), primarily in an east-west direction. *ISO* far-IR observations by RE96 measure this emission as a cold dust component (36 K),

consistent with dust heated in H II regions (Telesco, Becklin, & Wynn-Williams 1980). However, observations by Pérez-Fournon & Wilson (1990) in Hα show that these H II regions exist in an elliptical galactic bar at a radius of $\sim$50″ ($\sim$3 kpc) from the nucleus. Thus, these star-forming regions cannot contribute to the mid-IR emission that we observe within our $\sim$11″ field of view.

Star formation in the circumnuclear region of NGC 4151 has been characterized using the strength of polycyclic aromatic hydrocarbon (PAH) emission. Galaxies with strong nuclear star formation also feature strong PAH emission. This PAH emission, however, is found to be weak or absent in AGNs with weak star formation (Roche et al. 1991; Genzel et al. 1998). In the case of NGC 4151, Roche & Aitken (1985) and Imanishi et al. (1998) failed to detect PAH emission at 11.4 and 3.3 μm, respectively, with their $\sim$4″ apertures. Further observations by Sturm et al. (1999) also failed to detect any PAH emission at 11.2, 8.7, 7.7, or 6.2 μm. Thus, the mid-IR emission we observe on a scale of $\sim$3.″5 is unlikely to be associated with significant star formation.

4.3. *Dusty Narrow-Line Region*

The most likely explanation for the "extended" mid-IR morphology in NGC 4151 is emission from a dusty NLR (Rieke & Lebofsky 1981; RE96). Dust in this region has a direct view of the central engine and hence can be heated, resulting in extended mid-IR emission. The emission we observe follows the NLR, as delineated by the [O III] observations of Kaiser et al. (2000), lending support to this concept. Mid-IR emission coincident with [O III] NLR emission has also been observed in other galaxies, such as NGC 1068 (Braatz et al. 1993; Cameron et al. 1993) and Cyg A (Radomski et al. 2001, 2002). In both galaxies, dust heated by the central engine most likely contributes to this emission.

In order to explore the possibility of central heating, we calculated color temperatures based on the ratio of our 10.8 and 18.2 μm images. Temperature and emission optical depth maps from simple radiative transfer analysis provide a good first-order estimate of the sources of grain heating, as well as the relative density of warm grains (Tresch-Fienberg et al. 1987). Figure 4 shows our temperature and emission optical depth maps. We calculate color temperatures ranging from $\sim$185 $\pm$ 5 K in the core to $\sim$165 $\pm$ 15 K within the NLR ($r \sim 100$ pc), consistent with the warm dust component (170 K), as measured by *ISO* (RE96). The emission optical depth shows that the density of these dust grains is enhanced along the direction of the NLR. Assuming a simple uniform dust distribution, a first-order determination of the size of the region that could be heated by a central source can be made. Given that dust grains primarily absorb UV-optical radiation and reemit in the infrared, the equilibrium temperature of dust in a strong UV field is given by (Sellgren, Werner, & Dinerstein 1983)

$$T \sim \left(\frac{L_{\rm UV}}{16\pi R^2 \sigma}\frac{Q_{\rm UV}}{Q_{\rm IR}}\right)^{1/4}. \quad (1)$$

In the above equation, T is the dust temperature, $L_{\rm UV}$ is the UV luminosity of the central source, R is the radius from the source in parsecs, σ is the Stefan-Boltzmann constant, and $Q_{\rm UV}/Q_{\rm IR}$ is the ratio of the Planck-averaged UV absorption coefficient to the infrared emission coefficient.

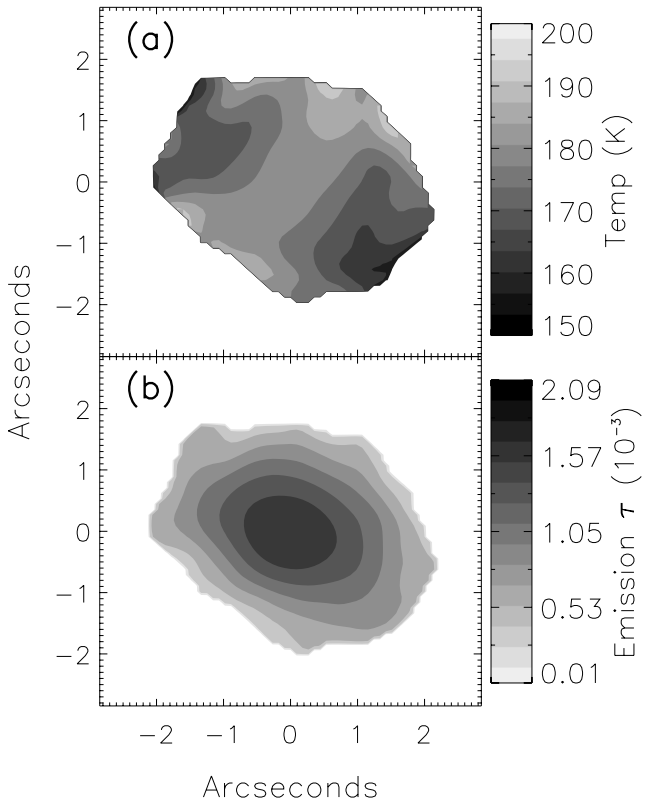

FIG. 4.—(*a*) Temperature and (*b*) emission optical depth map of the central $\sim$6″ of NGC 4151. Temperature peaks along the very outer edges are erroneous and most likely due to a low signal-to-noise ratio.

Values of $Q_{\rm UV}/Q_{\rm IR}$ are dependent on the dust grain size and composition and are given by Draine & Lee (1984), Laor & Draine (1993), and Weingartner & Draine (2001) for graphite and "smoothed astronomical" (SA) silicate.

The observed UV-optical luminosity of NGC 4151 is $\sim 10^{10}\ L_\odot$ (Penston et al. 1990). Given this luminosity, in order to heat dust to the observed temperature of $\sim$165 $\pm$ 15 K at a distance of $\sim$100 pc, the inner NLR should be composed of 0.004 μm graphite grains or 0.001 μm SA silicate grains. These grain sizes fall near or below the limit of classical interstellar dust grains that range from 0.003 to 1 μm (Draine & Lee 1984). They also are much smaller than the estimated grains sizes used for the centrally heated NLR models of NGC 1068 ($\sim$0.05 μm; Cameron et al. 1993) and Cyg A ($\sim$0.1 μm; Radomski et al. 2002). However, Penston et al. (1990) proposed that the continuum emission in NGC 4151 is inherently anisotropic and that the ionizing luminosity, as seen within the extended NLR (1–2 kpc), may be an order of 13 times greater than that observed from Earth. Subsequent models by Schulz & Komossa (1993), Yoshida & Ohtani (1993), and Robinson et al. (1994) also derive values for the anisotropy as high as 3–10. Thus, a better estimate of the luminosity in the NLR may be $\sim 10^{11}\ L_\odot$. This higher luminosity would increase the calculated grain sizes by an order of magnitude (0.04 μm graphite or 0.01 μm SA silicate), resulting in sizes more consistent with classical interstellar dust and grain size estimates in the NLRs of NGC 1068 and Cyg A. Thus, to first order, assuming that the luminosity in NGC 4151 is anisotropic, the extended mid-IR emission is consistent with heating of dust in the NLR from a central engine.

4.4. *Dusty Torus*

Another source of mid-IR emission in NGC 4151 may be from a dusty torus (RE96). Emission from a dusty torus may dominate the unresolved mid-IR component in NGC 4151. It is considered that we view this disk/torus through a line of sight passing near the boundary edge (Cassidy & Raine 1996). Assuming the torus lies perpendicular to the NLR, its major axis would be oriented in an approximately north-south direction. We see no extended emission in this direction and can only place an upper limit on the mid-IR size of the torus of $\lesssim 35$ pc, based on our resolution limit of $\sim 0\farcs53$–$0\farcs58$. This is consistent with the polarimetry observations and subsequent modeling of Ruiz et al. (2003), which suggest that the torus size in NGC 4151 is ≈ 30 pc. A direct measurement of the torus may have been made by N90. As previously mentioned, north-south scans by N90 measure the 11.2 μm emitting region to be $0\farcs16 \pm 0\farcs04$ or ~ 10 pc. Based on our "unresolved" (PSF) component, we therefore place an upper limit on the mid-IR contribution of a dusty torus of $\lesssim 73\%$ of the total emission at 10.8 and 18.2 μm. This represents the maximum contribution from a dusty torus and does not rule out contribution to the "unresolved "mid-IR emission from a self-absorbed synchrotron source.

Observations of neutral H I and molecular H_2 by Mundell et al. (1995) and Fernandez et al. (1999), respectively, show evidence of a gaseous disk up to $2\farcs5$ (160 pc), across which may be associated with the torus. This disk is located in approximately a north-south direction and may consist of an "onion-skin" morphology, as discussed by Pedlar et al. (1998). In this model, the gaseous torus contains several layers (see Fig. 5). The innermost ring consists of ionized gas, followed by a ring of neutral H I gas surrounded by a ring of molecular H_2. In Pedlar's "onion-skin" model, the authors further expand on the subject of anisotropy in NGC 4151, as discussed by Penston et al. (1990). Using observations of free-free absorption detected at 73 and 18 cm, in conjunction with observations of H I by Mundell et al. (1995), they estimate the ionizing flux incident on the torus. Assuming a simple Strömgren model, they calculate that the ionizing flux in the plane of the torus is between ~ 10 and 40 times less than seen from Earth or ~ 100–500 times less than seen in the NLR, as modeled by Penston et al. (1990).

To test the validity of this model, we can use the dust equilibrium equation from § 4.3. Given values for temperature and dust grain size discussed above, we can calculate the size of the mid-IR torus as a function of ionizing luminosity, $L_{\rm UV}$. Color temperature measurements of the core of NGC 4151 show $T \sim 185 \pm 5$ K. If the dusty torus intercepts the ionizing luminosity as seen from Earth $\sim 10^{10}\ L_\odot$ and consists of dust grains similar to those estimated for the NLR (0.04 μm graphite or 0.01 μm SA silicate), the size of the torus in the mid-IR would be $\sim 0\farcs65$ (~ 42 pc). This is slightly larger than the size of the torus, based on our resolution limit of $\sim 0\farcs53$–$0\farcs58$ ($\lesssim 35$ pc) and that of the Ruiz polarimetry model (≈ 30 pc). It is also 4 times larger than the north-south scans by N90, which measured the 11.2 μm emitting region to be $0\farcs16 \pm 0\farcs04$ or ~ 10 pc. Assuming the N90 mid-IR emission delineates the torus, dust grains in the torus would need to be ~ 10 times larger than those found in the NLR. Alternatively, if the luminosity in the plane of the torus is ~ 10–40 times less than seen from Earth, as modeled by Pedlar et al. (1998), the size of the torus in the mid-IR would range between $\sim 0\farcs1$ and $0\farcs2$ (~ 7–14 pc). Although slightly smaller than the Ruiz model, this size torus would be consistent with our upper limit as well as closely match the size measured by N90. Thus, the "onion-skin" model of Pedlar et al. (1998), which suggests that the luminosity in NGC 4151 may be very weak in the plane of the torus, is roughly consistent with size estimates of the torus in the

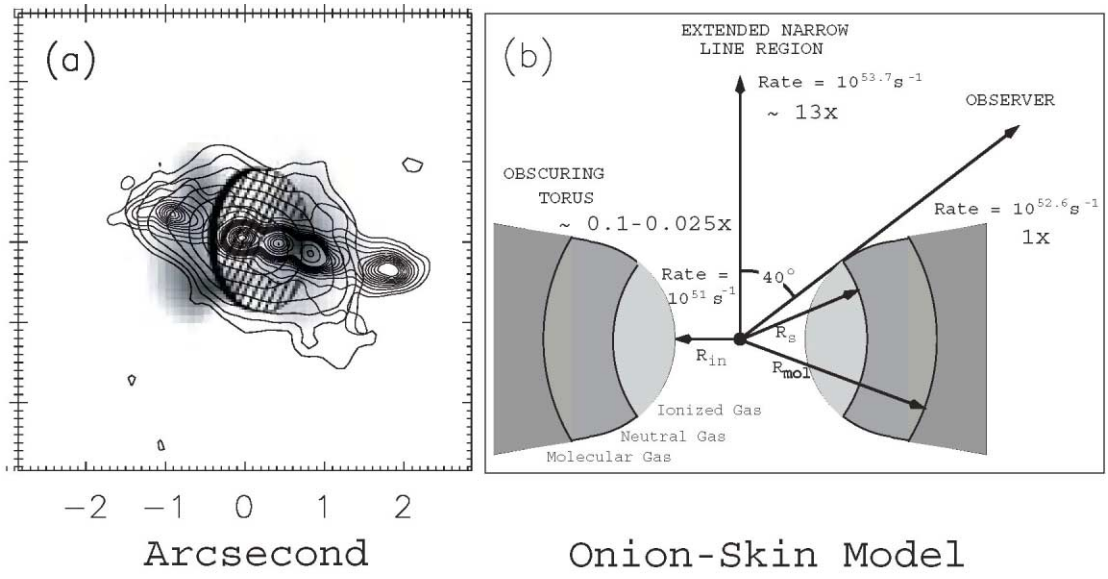

FIG. 5.—Image (*a*) shows four sets of data. First is the proposed H I disk from Mundell et al. (1995) (*cross-hatched disk*). Second is the molecular H_2 1–0 *S*(1) ring, as observed by Fernandez et al. (1999) (*gray scale*). Both these images are overlaid on the 18 cm radio image from Pedlar et al. (1998, *narrow contours*). Finally, the larger contours represent our 18.2 μm image from Fig. 2, with the subtracted PSF scaled to 80%. Image (*b*) shows the "onion-skin" model of the gaseous torus from Pedlar et al. (1998; their Fig. 6). The rate values are the ionizing photons per second, as calculated from Penston et al. (1990; NLR and Observer) and Pedlar et al. (1998; torus). The rate of 10^{51} s^{-1} is based on the lower limit from Pedlar et al. (1998). The upper limit is ~ 3 times greater, resulting in a range of ionizing flux 0.1–0.025 times as great as that observed from Earth.

mid-IR. However, it should be noted that the results discussed above derive from simple equations involving Strömgren radii and dust grains at equilibrium temperatures. Due to the increased density of material associated with the torus, as opposed to the NLR, a more robust radiative transfer analysis may be needed to truly understand the anisotropy in NGC 4151.

5. CONCLUSIONS

In this paper we have used mid-IR imaging and first-order radiative transfer analysis, assuming dust grains in thermal equilibrium, to study the central $\sim 11''$ of NGC 4151. Our conclusion are as follows.

1. We detect extended mid-IR emission at 10.8 and 18.2 μm in the circumnuclear region of NGC 4151. This emission extends approximately $\sim$200 pc ($\sim 3\farcs5$) at a P.A. $\sim 60^\circ$, correlating with the NLR region as seen in [O III] λ5007 by Evans et al. (1993) and Kaiser et al. (2000) using *HST*.

2. With the PSF scaled to 100% of the peak of NGC 4151, we measure limits to the unresolved and resolved components of $\leq$73% and $\geq$27%, respectively.

3. Mid-IR line emission contributes less than 10% of the extended emission at 10.8 and 18.2 μm. The lack of any detectable PAH emission also shows that star formation is weak in the circumnuclear region.

4. Assuming that the luminosity in NGC 4151 is anisotropic ($\sim$13 times), the extended mid-IR emission in NGC 4151 is consistent with thermal reradiation from dust grains in the NLR heated by a central engine.

5. We place an upper limit on the size of the torus in the mid-IR of $\lesssim$35 pc, consistent with the measurements of N90 and Ruiz et al. (2003). This results in an upper limit to the mid-IR contribution from a dusty torus in NGC 4151 of $\leq$73% of the total emission at 10.8 and 18.2 μm, based on our unresolved (PSF) component.

6. Mid-IR measurements of the proposed torus by N90, as well as upper limits derived from this paper, are roughly consistent with the "onion-skin" model of Pedlar et al. (1998). In this model, ionizing photons in the plane of the torus may be $\sim$10–40 times fewer than seen from Earth.

We would like to thank the Florida Space Grant Consortium for funding that led to the completion of this work, as well as engineer Chris Carter, who provided invaluable support while these observations were taken at Gemini North.

REFERENCES

Ayani, K., & Maehara, H. 1991, PASJ, 43, L1
Braatz, J. A., Wilson, A. S., Gezari, D. Y., Varosi, F., & Beichman, C. A. 1993, ApJ, 409, L5
Cameron, M., Storey, J. W. V., Rotaciuc, V., Genzel, R., Verstraete, L., Drapatz, S., Siebenmorgen, R., & Lee, T. J. 1993, ApJ, 419, 136
Carleton, N. P., Elvis, M., Fabbiano, G., Willner, S. P., Lawrence, A., & Ward, M. 1987, ApJ, 318, 595
Cassidy, I., & Raine, D. J. 1996, A&A, 310, 49
Clavel, J., et al. 1990, MNRAS, 246, 668
Cohen, M., Witteborn, F. C., Walker, R. G., Bregman, J. D., & Wooden, D. H. 1995, AJ, 110, 275
Contini, M., Viegas, S. M., & Prieto, M. A. 2002, A&A, 386, 399
Crenshaw, D. M., Kraemer, S. B., Hutchings, J. B., Bradley, L. D., 11, Gull, T. R., Kaiser, M. E., Nelson, C. H., Ruiz, J. R., & Weistrop, D. 2000, AJ, 120, 1731
de Kool, M., & Begelman, M. C. 1989, Nature, 338, 484
Dopita, M. A., & Sutherland, R. S. 1996, ApJS, 102, 161
Draine, B. T. 1981, ApJ, 245, 880
Draine, B. T., & Lee, H. M. 1984, ApJ, 285, 89
Edelson, R. A., & Malkan, M. A. 1986, ApJ, 308, 59
Edelson, R. A., Malkan, M. A., & Rieke, G. H. 1987, ApJ, 321, 233
Engargiola, G., Harper, D. A., Elvis, M., & Willner, S. P. 1988, ApJ, 332, L19
Evans, I. N., Tsvetanov, Z., Kriss, G. A., Ford, H. C., Caganoff, S., & Koratkar, A. P. 1993, ApJ, 417, 82
Fernandez, B. R., Holloway, A. J., Meaburn, J., Pedlar, A., & Mundell, C. G. 1999, MNRAS, 305, 319
Fitch, W. S., Pacholczyk, A. G., & Weymann, R. J. 1967, ApJ, 150, L67
Genzel, R., et al. 1998, ApJ, 498, 579
Imanishi, M., Terada, H., Goto, M., & Maihara, T. 1998, PASJ, 50, 399
Johnston, K. J., Elvis, M., Kjer, D., & Shen, B. S. P. 1982, ApJ, 262, 61
Kaiser, M. E., et al. 2000, ApJ, 528, 260
Laor, A., & Draine, B. T. 1993, ApJ, 402, 441
Lyutyi, V. M. 1972, AZh, 49, 930
Mundell, C. G., Pedlar, A., Baum, S. A., O'Dea, C. P., Gallimore, J. F., & Brinks, E. 1995, MNRAS, 272, 355
Neugebauer, G., Graham, J. R., Soifer, B. T., & Matthews, K. 1990, AJ, 99, 1456 (N90)
Osterbrock, D. E., & Koski, A. T. 1976, MNRAS, 176, 61P
Papadakis, I. E., & McHardy, I. M. 1995, MNRAS, 273, 923
Pedlar, A., Fernandez, B., Hamilton, N. G., Redman, M. P., & Dewdney, P. E. 1998, MNRAS, 300, 1071
Pedlar, A., Kukula, M. J., Longley, D. P. T., Muxlow, T. W. B., Axon, D. J., Baum, S., O'Dea, C., & Unger, S. W. 1993, MNRAS, 263, 471
Penston, M. V., & Perez, E. 1984, MNRAS, 211, 33P
Penston, M. V., et al. 1990, A&A, 236, 53
Perez-Fournon, I., & Wilson, A. S. 1990, ApJ, 356, 456
Radomski, J. T., Piña, R. K., Packham, C., Telesco, C. M., & Tadhunter, C. N. 2001, in ASP Conf. Ser. 249, The Central Kiloparsec of Starbursts and AGN: The La Palma Connection, ed. J. H. Knapen, J. E. Beckman, I. Shlosman, & T. J. Mahoney (San Francisco: ASP), 325
———. 2002, ApJ, 566, 675
Rieke, G. H., & Lebofsky, M. J. 1981, ApJ, 250, 87
Rieke, G. H., & Low, F. J. 1972, ApJ, 177, L115
Robinson, A., et al. 1994, A&A, 291, 351
Roche, P. F., & Aitken, D. K. 1985, MNRAS, 215, 425
Roche, P. F., Aitken, D. K., Smith, C. H., & Ward, M. J. 1991, MNRAS, 248, 606
Rodriguez Espinosa, J. M., Perez Garcia, A. M., Lemke, D., & Meisenheimer, K. 1996, A&A, 315, L129 (RE96)
Ruiz, M., Young, S., Packham, C., Alexander, D. M., & Hough, J. H. 2003, MNRAS, in press.
Schulz, H., & Komossa, S. 1993, A&A, 278, 29
Sellgren, K., Werner, M. W., & Dinerstein, H. L. 1983, ApJ, 271, L13
Sturm, E., Alexander, T., Lutz, D., Sternberg, A., Netzer, H., & Genzel, R. 1999, ApJ, 512, 197
Telesco, C. M. 1988, ARA&A, 26, 343
Telesco, C. M., Becklin, E. E., & Wynn-Williams, C. G. 1980, ApJ, 241, L69
Tresch-Fienberg, R., Fazio, G. G., Gezari, D. Y., Lamb, G. M., Shu, P. K., Hoffmann, W. F., & McCreight, C. R. 1987, ApJ, 312, 542
Turner, J. E. H., Allington-Smith, J., Chapman, S., Content, R., Done, C., Haynes, R., Lee, D., & Morris, S. 2002, MNRAS, 331, 284
Ward, M., Elvis, M., Fabbiano, G., Carleton, N. P., Willner, S. P., & Lawrence, A. 1987, ApJ, 315, 74
Weingartner, J. C., & Draine, B. T. 2001, ApJ, 548, 296
Yoshida, M., & Ohtani, H. 1993, PASJ, 45, 407